ISSN 1674-1056
http://cpb.iphy.ac.cn
http://iopscience.iop.org/cpb
中国物理 B
Chinese Physics
中国物理 Chinese Physics B

In situ formed FeS_2@CoS cathode for long cycling life lithium-ion battery

Xin Wang(王鑫), Bojun Wang(汪博筠), Jiachao Yang(杨家超), Qiwen Ran(冉淇文), Jian Zou(邹剑), Pengyu Chen(陈鹏宇), Li Li(李莉), Liping Wang(王丽平), and Xiaobin Niu(牛晓滨)

Citation: Chin. Phys. B, 2021, 30 (**8**): 088201. DOI: 10.1088/1674-1056/abe9ab
Journal homepage: http://cpb.iphy.ac.cn; http://iopscience.iop.org/cpb

What follows is a list of articles you may be interested in

Electron density distribution of $LiMn_2O_4$ cathode investigated by synchrotron powder x-ray diffraction

Tongtong Shang(尚彤彤), Dongdong Xiao(肖东东), Qinghua Zhang(张庆华), Xuefeng Wang(王雪锋), Dong Su(苏东), and Lin Gu(谷林)

Chin. Phys. B, 2021, 30 (**7**): 078202. DOI: 10.1088/1674-1056/abf347

Silicon micropillar electrodes of lithiumion batteries used for characterizing electrolyte additives

Fangrong Hu(胡放荣), Mingyang Zhang(张铭扬), Wenbin Qi(起文斌), Jieyun Zheng(郑杰允), Yue Sun(孙悦), Jianyu Kang(康剑宇), Hailong Yu(俞海龙), Qiyu Wang(王其钰), Shijuan Chen(陈世娟), Xinhua Sun(孙新华), Baogang Quan(全保刚), Junjie Li(李俊杰), Changzhi Gu(顾长志), and Hong Li(李泓)

Chin. Phys. B, 2021, 30 (**6**): 068202. DOI: 10.1088/1674-1056/abf558

DFT study of solvation of Li^+/Na^+ in fluoroethylene carbonate/vinylene carbonate/ethylene sulfite solvents for lithium/sodium-based battery

Qi Liu(刘琦, Guoqiang Tan(谭国强), Feng Wu(吴锋), Daobin Mu(穆道斌), and Borong Wu(吴伯荣)

Chin. Phys. B, 2021, 30 (**3**): 038203. DOI: 10.1088/1674-1056/abd763

Understanding the Li diffusion mechanism and positive effect of current collector volume expansion in anode free batteries

Yan Zhuang(庄严), Zheyi Zou(邹喆义), Bo Lu(吕涛), Yajie Li(李亚捷), Da Wang(王达), Maxim Avdeev, Siqi Shi(施思齐)

Chin. Phys. B, 2020, 29 (**6**): 068202. DOI: 10.1088/1674-1056/ab943c

First-principles insight into Li and Na ion storage in graphene oxide

Shu-Ying Zhong(钟淑英), Jing Shi(石晶), Wen-Wei Luo(罗文崴), Xue-Ling Lei(雷雪玲)

Chin. Phys. B, 2019, 28 (**7**): 078201. DOI: 10.1088/1674-1056/28/7/078201

In situ formed FeS_2@CoS cathode for long cycling life lithium-ion battery*

Xin Wang(王鑫)[1], Bojun Wang(汪博筠)[1], Jiachao Yang(杨家超)[1], Qiwen Ran(冉淇文)[1], Jian Zou(邹剑)[1], Pengyu Chen(陈鹏宇)[1], Li Li(李莉)[1], Liping Wang(王丽平)[1,2,†], and Xiaobin Niu(牛晓滨)[1,‡]

[1] *School of Materials and Energy, University of Electronic Science and Technology of China, Chengdu* 611731, *China*
[2] *Tianmu Lake Institute of Advanced Energy Storage Technologies, Changzhou* 213300, *China*

(Received 17 December 2020; revised manuscript received 29 January 2021; accepted manuscript online 25 February 2021)

Pyrite FeS_2 exhibits an ultrahigh energy density (1671 W·h·kg^{-1}, for the reaction of $FeS_2 + 4Li = Fe + 2Li_2S$) in secondary lithium-ion batteries, but its poor cycling stability, huge volume expansion, the shuttle effect of polysulfides, and slow kinetic properties limit its practical application. In this work, we synthesize a composite structure material CoS on FeS_2 surface (FeS_x@CoS, $1 < x \leq 2$) by using a cobalt-containing MOF to improve its cycle stability. It is found that CoS inhibits the side reactions and adsorbs polysulfides. As a result, the modified FeS_2 shows a higher discharge capacity of 577 mA·h·g^{-1} (919 W·h·kg^{-1}) after 60 cycles than 484 mA·h·g^{-1} (778 W·h·kg^{-1}) of bare pyrite FeS_2. This efficient strategy provides a valuable step toward the realization of high cycling stability FeS_2 cathode materials for secondary lithium-ion batteries and enriches the basic understanding of the influence of FeS_2 interfacial stability on its electrochemical performances.

Keywords: Li-free cathodes, pyrite, lithium metal batteries, first-principles calculation

PACS: 82.47.Aa, 82.45.Fk, 31.15.A– **DOI:** 10.1088/1674-1056/abe9ab

1. Introduction

At present, as the energy density of conventional lithium-ion battery (LIB) electrode materials is approaching their limit, the next-generation electrode materials are needed to meet the demand for cheap, safety, and high-energy density.[1–6] Pyrite FeS_2 is considered as a promising candidate of cathode materials due to its advantages of high energy capacity (1671 W·h·kg^{-1}), low price, and environmentally sustainability.[7–10] In our previous study, we revealed that the cycling performance of FeS_2 was extremely limited by shuttle effects of polysulfides (PS, Li_2S_n with $n > 2$), and huge volume variations.[11,12] In particular, the shuttle effect mainly causes the loss of active materials, leading to a rapid capacity degradation. Therefore, it is important to solve and suppress the shuttle effect.

In recent years, researchers have explored different strategies to inhibit the dissolution and shuttle of polysulfides.[13–17] It is found that using an electrolyte with low polysulfide solubility to reduce polysulfide solubility is an effective way.[18] Chen and co-workers[16] found that FeS_2 exhibits better electrochemical performance in ether-based diglyme (DGM) electrolyte than in ethylene carbonate/diethyl carbonate (EC/DEC) electrolyte, due to the significant suppression of the side reactions from DGM. In addition, the polysulfide adsorption materials play an extremely important role in controlling the shuttle effect. Yi *et al.*[19] demonstrated that polar oxides, sulfides, and carbides have strong chemical bonds with polysulfides, which can synergistically achieve controlling of the dissolution of polysulfides and the promotion of the utilization of sulfur. They proved that VS_2-, TiS_2-, and CoS_2-based materials show higher binding energies with polysulfides, lower diffusion and activation energy barrier, thereby increasing the discharge capacity and cycling stability. Arumugam *et al.*[14] investigated that Co_9S_8 can not only adsorb polysulfides through bonding, but also improve the electronic conductivity. However, the polysulfide adsorbent mentioned above is only used in Li-S batteries, not used in Li-FeS_2 secondary batteries. Noticeably, it is more complicated and difficult to suppress the shuttle effect of polysulfides in Li-FeS_2 batteries than in Li-S batteries because of the additional dissolution of Fe.[20]

Metal-organic framework (MOF) materials have been widely used in lithium-ion batteries due to their large specific surface area, porous, and adjustable structure. It has been proved that MOF is an effective template/precursor for metal-based and carbon-based nanocomposites.[21] Various MOF-derived materials obtained by using MOF as a self-sacrificing template not only retain porous structures, but also exhibit excellent electronic conductivity, thus leading to the improve-

*Project supported by the Fundamental Research Funds for the Central Universities, China (Grant No. ZYGX2019Z008) and the National Natural Science Foundation of China (Grant No. 52072061).

†Corresponding author. E-mail: lipingwang@uestc.edu.cn
‡Corresponding author. E-mail: xbniu@uestc.edu.cn

© 2021 Chinese Physical Society and IOP Publishing Ltd

ment of the cycling performance and rate performance.[22]

In this work, we use a one-pot synthesis method to *in situ* form a FeS_x@CoS composite cathode material to reduce the adverse effects of polysulfide shuttle effect and to improve its electrochemical performance. The FeS_x@CoS originates from a calcination of FeS_2 and ZIF-67[23] (mainly $C_8H_{12}N_4Co$, Co-based zeolitic imidazolate framework materials) mixture. The mixture is uniformly embedded on the surface of FeS_2. Through a heat treatment, a protective layer of CoS is *in situ* formed on the surface of FeS_2. The protective layer utilizes the strong adsorption ability of CoS for lithium polysulfide and the high specific area to prevent side reactions. As a result, we have improved the cycle stability of FeS_2.

2. Experimental details

2.1. Synthesis of Co-NC450

In a typical preparation, 2 mmol of $Co(NO_3)_2{\cdot}6H_2O$ and 8 mmol of 2-methylimidazole ($C_4H_6N_2$) were separately dissolved in 25 mL of methanol. Then, 2-methylimidazole solution was slowly added dropwise to $Co(NO_3)_2{\cdot}6H_2O$ solution with continuous magnetic stirring. After stirring for 6 hours, the solution was aged for 18 hours at room temperature. The purple precipitate after filtration was washed three times with absolute ethanol and dried in a vacuum oven at 60 °C for 6 h. Then, a purple ZIF-67 product was obtained. It was calcined in a nitrogen atmosphere at 450 °C for 3 hours. Finally, black powders were obtained, named as Co-NC450.

2.2. Synthesis of 1%-FeS_x@CoS.

We took 600 mg pristine FeS_2 (from the Tianmu Lake Institute of Advanced Energy Storage Technologies) and 227 mg $Co(NO_3)_2{\cdot}6H_2O$, and added them into 6 mL of methanol. The mixed solution was stirred for 30 min, named as solution A. Meanwhile, 256 mg of 2-methylimidazole was dissolved in 6 mL of methanol solution, named as solution B. Solution B was slowly added dropwise into solution A, and then stirred for 6 hours, and then aged for 18 hours. Thus, we got the precipitation named as ZIF-FeS_2. After washing and drying, ZIF-FeS_2 was heated in a nitrogen atmosphere at 450 °C for 3 hours. Finally, black powders (named as 1%-FeS_x@CoS) were obtained. The Co can be tuned and determined by inductively coupled plasma optical emission spectrometer (ICP-OES) analysis (Table S1).

2.3. Synthesis of Li_2S_6 solution

The Li_2S_6 solution was prepared following a previously work.[15] Sulfur (S_8) power and lithium sulfide (Li_2S) power were mixed uniformly in argon atmosphere at a molar ratio of 3:4. Then 1,3-dioxolane (DOL)/1,2-dimethoxyethane (DME) solvent with a volume ratio of 1:1 was added to the mixture. Finally, a brown Li_2S_6 solution was obtained after stirring at 50 °C for 12 hours.

2.4. Calculation method

The binding energies of Li_2S_6 on CoS, FeS_2, and Fe_7S_8 were estimated by density functional theory (DFT) calculations. All the spin-polarized calculations were developed by Vienna *ab initio* simulation package (VASP),[24,25] software package with projector-augmented wave (PAW)[26] pseudopotentials. Exchange and correction interactions were described using the Perdew–Burke–Ernzerhof (PBE) functional.[27] The kinetic energy cutoff of plane waves was optimized and set to 500 eV and the energy convergence threshold of self-consistent field (SCF) calculation was 10^{-6} eV. The *k*-point grids used in Brillouin zone sampling during SCF calculation are carefully tested for the bulk structures and corresponding supercell slab models. Supercell slab models were built for CoS (001), FeS_2 (001), and Fe_7S_8 (100) surface. A 20 Å vacuum layer was reserved between two periodic slabs for avoiding neighboring interactions, and bottom layer atoms were fixed to corresponding optimized bulk configurations. All structures were fully relaxed until residual forces within 10^{-2} eV·Å^{-1}.

3. Results and discussion

Figure 1 illustrates the preparation process of the FeS_x@CoS composite. Firstly, $Co(NO_3)_2{\cdot}6H_2O$ and pristine FeS_2 are mixed uniformly in a methanol solution to fabricate a homogeneous ZIF-67 embedded FeS_2 product. The ZIF-67 is converted in Co metal and nitrogen doped carbon first, then form CoS through reaction with FeS_2 heat treatment. Finally, FeS_x@CoS composite is obtained.

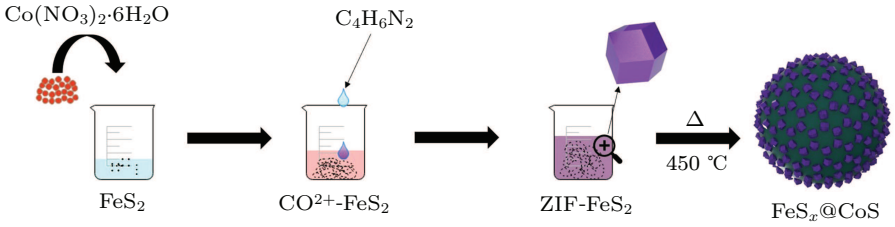


Fig. 1. Schematic illustration of the preparation of FeS_x@CoS.

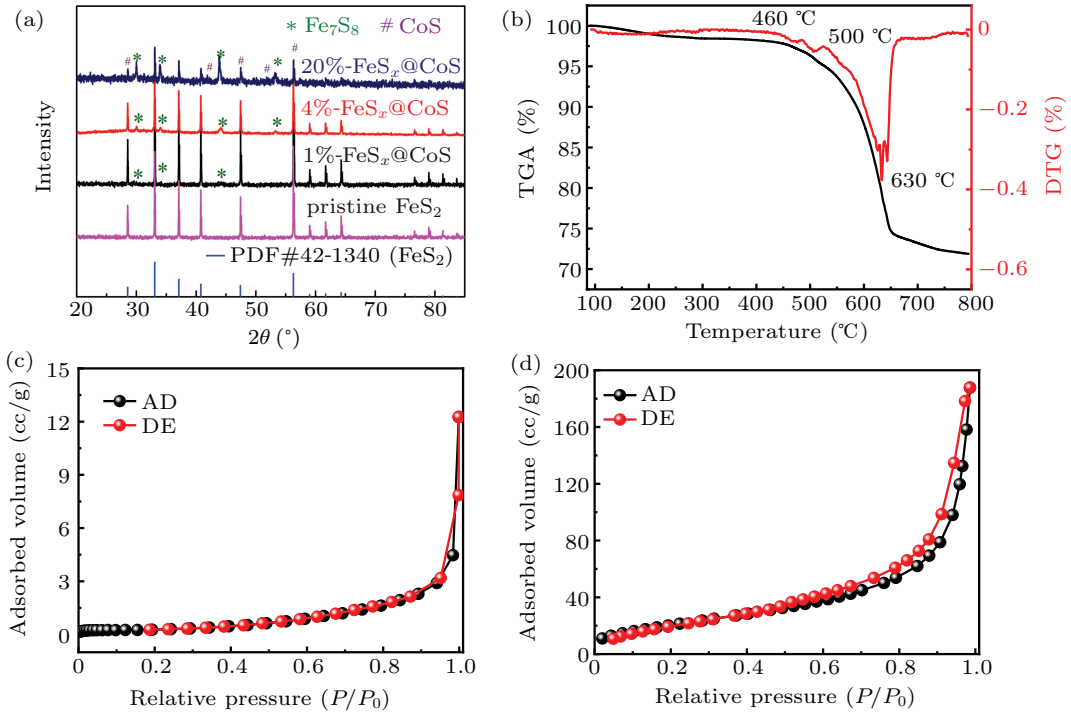


Fig. 2. (a) XRD patterns of pristine FeS_2, 1%-FeS_x@CoS, 4%-FeS_x@CoS and 20%-FeS_x@CoS; (b) thermogravimetric curve of 1%-FeS_x@CoS under N_2 atmosphere at a heating rate of 10 °C/min; N_2 adsorption–desorption isotherms of (c) pristine FeS_2; (d) Co-NC450.

X-ray diffraction (XRD) is applied to confirm the crystal structure of FeS_x@CoS with different amounts of $Co(NO_3)_2{\cdot}6H_2O$. As shown in Fig. 2(a), the main diffractions peaks are identified to pyrite FeS_2 (standard JCPDS card No. 42-1340). Fe_7S_8 (standard JCPDS card No. 29-0723) is also observed. This can be explained that the cobalt atoms in ZIF-67 capture S_2^{2-} in FeS_2. CoS characteristic peaks are not evident mainly due to a low cobalt content. With the increasing amount of cobalt, the characteristic peak of CoS appears in 20%-FeS_x@CoS. In Fig. 2(b), the TGA curve of 1%-FeS_x@CoS demonstrates that the interaction between ZIF-67 and FeS_2 occurs at about 450 °C. The large weight loss at 630 °C may be caused by the thermal decomposition of FeS_2 to Fe_7S_8. Figures 2(c) and 2(d) show the nitrogen adsorption and desorption isotherms of pristine FeS_2 and Co-NC450 (calcined ZIF-67). The specific surface area of pristine FeS_2 is only about 1.0 $m^2{\cdot}g^{-1}$. The adsorption curve of Co-NC450 has a small hysteresis in the P/P_0 range of 0.8–1.0, which can be confirmed as type IV isotherm.[28–30] The corresponding BET surface area of Co-NC450 is about 79.2 $m^2{\cdot}g^{-1}$. The BET surface area of Co-NC is not much different from similar materials (Co_9S_8/N-C) reported previously.[21] Furthermore, this suggests that *in situ* formed CoS can improve the surface area of FeS_2.

The morphologies of the as-synthesized materials are studied by SEM measurements. In Fig. 3(a), ZIF-67 has rhombic dodecahedron shape in sizes of about 500 nm. Figure 3(b) shows that the interior of Co-NC450 has a hollow structure with aggregated small particles. The size of the pristine FeS_2 is about 10–20 μm (Fig. 3(c)). The SEM images of 1%-FeS_x@CoS in Figs. 3(d) and S1(a) confirm that the cobalt compound is sufficiently covered on the surface of FeS_2. In Fig. S1(b), the rhombic dodecahedron structure of cobalt compound is embedded in FeS_2. Here 4%-FeS_x@CoS (Figs. S1(c) and S1(d)) and 1%-FeS_x@CoS powders have similar morphologies. However, with increasing amount of cobalt, the material structure has changed significantly. In 20%-FeS_x@CoS, the FeS_2 is connected by ZIF-derived materials, demonstrating a huge particle to be ∼ 100 μm (Figs. S1(e) and S1(f)).

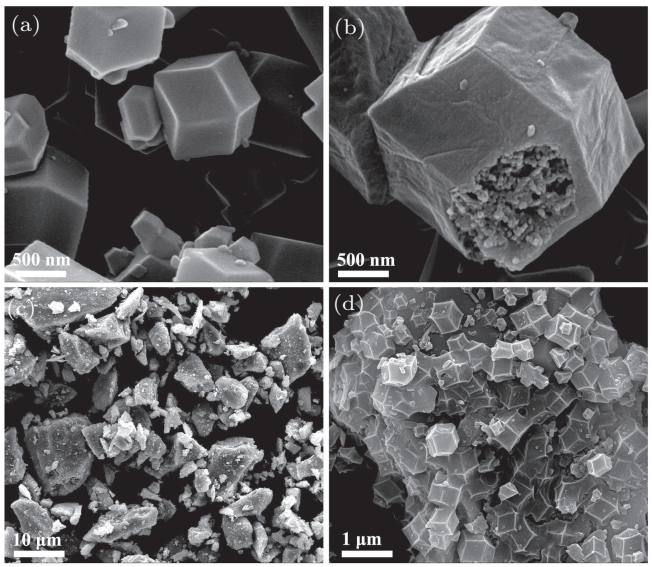


Fig. 3. SEM images of (a) ZIF-67, (b) Co-NC450, (c) pristine FeS_2, and (d) 1%-FeS_x@CoS.

The main characteristic XPS peaks of Fe are of Fe^{2+} in

1%-FeS_x@CoS (Fig. 4(a)), which Fe^{2+} peaks appear in the Fe 2p spectrum located at 707.1 eV (Fe^{2+} $2p_{3/2}$) and 719.9 eV (Fe^{2+} $2p_{1/2}$),[29,31,32] Fe^{3+} is also detected, which is due to a tiny iron oxidation. The XPS spectrum of Co 2p is shown in Fig. 4(b), which is assigned to Co^{2+} $2p_{3/2}$ of CoS (778.6 eV), Co^{2+} $2p_{1/2}$ of CoS (794.8 eV), Co^{2+} $2p_{3/2}$ of CoO (780.8 eV), Co^{2+} $2p_{1/2}$ of CoO (796.8 eV) and satellite peaks (784.7 eV, 803.1 eV).[21,28] This fully illustrates that Co-NC450 is converted to CoS on the surface of FeS_2 at high temperature. The appearance of the characteristic peaks of Co–O indicates that cobalt atoms on the surface are partially oxidized. The full XPS survey spectrum (Fig. S2(a)) shows that the main components of the 1%-FeS_x@CoS also include S, C, N, and O. As shown in Fig. S2(b), the characteristic peaks of S can be divided into the following five peaks,[28,33] at 161.2 eV (S $2p_{3/2}$ of S^{2-}), at 162.4 eV (S $2p_{1/2}$ of S^{2-}), at 163.7 eV (S $2p_{1/2}$ of S_2^{2-}), at 165.6 eV (C–S) and at 168.3 eV (SO_x), which reflect that CoS and Fe_7S_8 are formed on FeS_2.[28,33] Furthermore, the C element mainly exists in the form of C–S, C–N, and C–C/C=C (Fig. S2(c)).[33] The N element is mainly from pyridinic N, pyrrolic N, and graphic N (Fig. S2(d)).[34,35] The TEM shows a 1%-FeS_x@CoS surface structure, which further proves that the surface has nanosized rhombic dodecahedron structure (Fig. 4(c)). The micro-structure of the 1%-FeS_x@CoS composite material is further characterized by high-resolution transmission electron microscopy (HRTEM) (Fig. 4(d)). The interplanar distances of 0.242 nm, 0.264 nm, and 0.168 nm correspond to the (200) plane of FeS_2, the (004) plane of Fe_7S_8, and the (2$\bar{1}$0) plane of CoS, respectively, which are consistent with the results of XRD and XPS analyses.

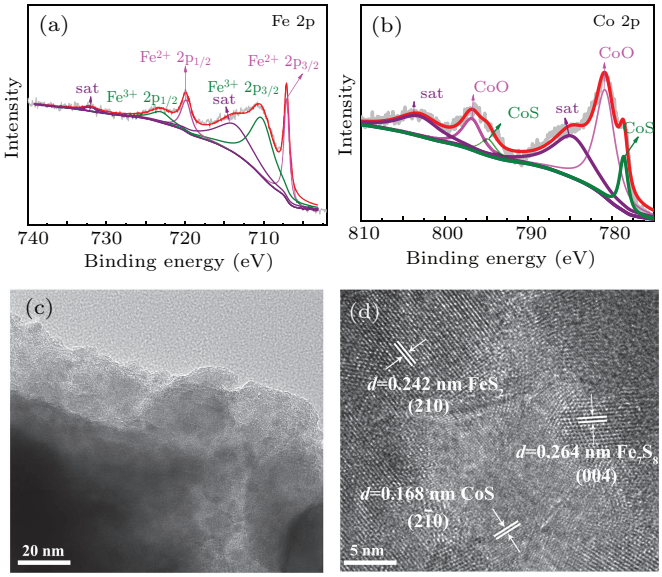


Fig. 4. XPS spectra of (a) Fe 2p, and (b) Co 2p; (c) TEM and (d) HRTEM images of the 1%-FeS_x@CoS.

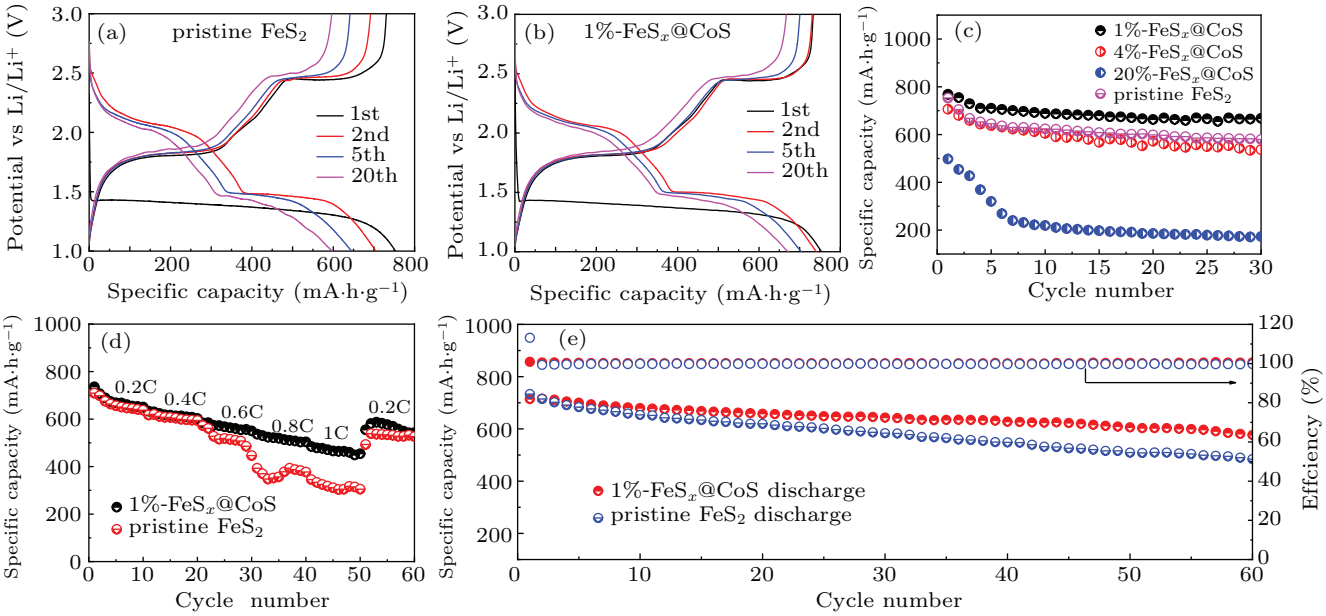


Fig. 5. The discharge/charge curves of (a) pristine FeS_2, and (b) 1%-FeS_x@CoS; (c) cyclic performance of different Co compounding amounts and pristine FeS_2 at 0.2 C rate; (d) rate performance of pristine FeS_2 and 1%-FeS_x@CoS; (e) the cycling performance of 1%-FeS_x@CoS and pristine FeS_2 at 0.5 C rate.

The electrochemical properties of FeS_x@CoS are demonstrated in Fig. 5. The voltage profiles of pristine FeS_2 and 1%-FeS_x@CoS are given in Figs. 5(a) and 5(b), respectively. In the initial discharge, there is only a plateau around 1.5 V, which corresponds to the conversion of FeS_2 to Fe and Li_2S. The charge curves include two plateaus at about 1.8 and 2.4 V, corresponding to $Fe + Li_2S \rightarrow FeS$ and $Li_2S \rightarrow S$, respectively.[11] In the second discharge, there are two discharge platforms including 2.3 V and 1.5 V, corresponding to $S \rightarrow Li_2S_n$ $(4 < n \leq 8) \rightarrow Li_2S$ and $FeS \rightarrow Li_2S + Fe$, respectively. This is consistent with the redox behavior of CV (Figs. S3(a) and S3(b)). The charging and discharging plat-

forms of as-prepared electrodes are not much different, indicating that the CoS has little influence on the bulk structure and discharge capacity. The discharge specific capacity at first cycle is similar in 1%-FeS_x@CoS and pristine FeS_2 as a small amount of CoS. Figure 5(c) demonstrates the influence of cobalt-containing on its cycling performance. Specifically, the reversible capacity of 1%-FeS_x@CoS and pristine FeS_2 electrodes are 668 and 580 mA·h·g^{-1} after 30 cycles at 0.2 C (1 C = 894 mA·g^{-1}), and the corresponding capacity retention are 86.9% and 76.9%, respectively. Its electrochemical performance has improved in comparison with the reported works.[36,37] The CoS protective layer on the surface of 1%-FeS_x@CoS successfully inhibit the shuttle effect of polysulfides and improve the stability of electrochemical cycles. However, with the increase of cobalt, the discharge capacity and cycling stability continues to decrease. As Co-NC450 only exerts the capacity of ~120 mA·h·g^{-1} (Fig. S3(c)). Moreover, the excessive compounding of cobalt on the surface will greatly affect the diffusion of lithium ions, which will reduce the stability. Figure 5(d) shows the superior rate performance of 1%-FeS_x@CoS compared to the pristine FeS_2 as the high specific surface area of CoS on the surface of 1%-FeS_x@CoS improves the electronic conductivity. To highlight the improvement of electrochemical performance, Fig. 5(e) provides a comparison of the cycle performance of 1%-FeS_x@CoS and pristine FeS_2 at 0.5 C rate. Here, 1%-FeS_x@CoS still maintains a specific capacity of 577 mA·h·g^{-1} after 60 cycles, with a retention rate of 81%. Pristine FeS_2 has only 484 mA·h·g^{-1} capacity remaining, and its retention rate is 66%. The initial Coulomb efficiency of 1%-FeS_x@CoS and pristine FeS_2 are 100.9% and 113.2%, respectively. The initial Coulomb efficiency greater than 100% is the result of the shuttle effect.[38] Pristine FeS_2 does cause poor electrochemical performance due to its shuttle effect of polysulfides. Furthermore, the compounding of CoS on pyrite FeS_2 has a beneficial effect on the inhibition of polysulfide shuttle effect.

To verify the adsorption effect of 1%-FeS_x@CoS on polysulfides, we put 1%-FeS_x@CoS in a Li_2S_6 solution, and observe its color changing. From Fig. 6(a), after 1 hour rest the original brown-yellow solution became transparent. This phenomenon proves that the 1%-FeS_x@CoS material has a strong adsorption effect on polysulfides. To further explore the interaction between lithium polysulfide and 1%-FeS_x@CoS, first-principles simulations are used. Figure 6(b) shows the original molecular configuration of Li_2S_6. Here 1%-FeS_x@CoS mainly includes three transition metal sulfides: FeS_2, CoS, and Fe_7S_8. The adsorption bond energy of the three types of transition metal sulfides with Li_2S_6 is used to estimate the adsorption effect of 1%-FeS_x@CoS on polysulfides. Figures 6(c)–6(e) show the adsorption configuration and adsorption binding energy of lithium polysulfide with different metal sulfides. In both CoS and Fe_7S_8 adsorption models, Li atoms of Li_2S_6 form bonds with S of metal sulfides. As for FeS_2, Fe atoms bond with S atoms of Li_2S_6 and S atoms bond to Li. The reason is that in the FeS_2 model, the surface Fe and S are basically on the same plane. In addition, part of Fe atoms have dangling bonds on the surface of FeS_2. The bond energy ΔE is calculated to express the adsorption energy of Li_2S_6 and different metal sulfides. The ΔE in the adsorption model can be calculated from the energy difference between the Li_2S_6-transition metal adsorption system and the sum of pure Li_2S_6($E_{Li_2S_6}$) and pure metal sulfides (E_{sub}), expressed as $\Delta E = E_{sub} + E_{Li_2S_6} - E_{sub+Li_2S_6}$ (a positive bond energy means that it is beneficial to adsorption).[19] Through calculation, the adsorption binding energies of Li_2S_6 with CoS, Fe_7S_8, and FeS_2 are 3.78 eV, 1.89 eV, and 1.44 eV, respectively. This proves that the formation of 1%-FeS_x@CoS is beneficial to the adsorption of polysulfides. This is consistent with the previous reports that transition metal sulfides have an adsorption effect on polysulfides.[19,39]

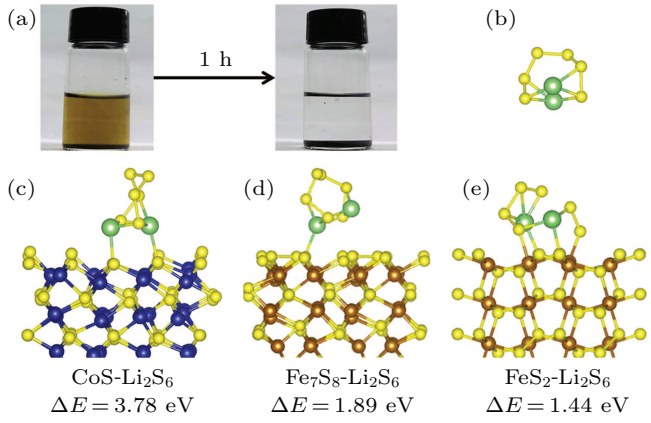


Fig. 6. (a) 1%-FeS_x@CoS placed in Li_2S_6 DOL/DME solution before and after the color contrast of the solution; (b) molecular configuration for Li_2S_6; the configuration and binding energy of Li_2S_6 adsorbed on (c) CoS, (d) Fe_7S_8 and (e) FeS_2. Here, blue, yellow, green, brown balls represent cobalt, sulfur, lithium and iron atoms, respectively.

4. Conclusions

In summary, a FeS_x@CoS compound has been successfully synthesized using the cobalt-containing MOF to react with pyrite FeS_2. The 1%-FeS_x@CoS electrode exhibits excellent cycling stability and rate performance. Specifically, it can maintain a discharge capacity of 577 mA·h·g^{-1} after 60 cycles, corresponding to an ultrahigh energy density of 919 W·h·kg^{-1}. The improvement of the cycling stability of the 1%-FeS_x@CoS electrode is mainly attributed to the formation of a high specific surface area CoS layer, which adsorbs lithium polysulfide and prevents the side reactions. This modification strategy effectively enhances the cycling performance of Li-FeS_2 secondary batteries and highlights the key role of interfacial stability for the robust FeS_2 cathode materials.

References

[1] Nitta N, Wu F, Lee J T and Yushin G 2015 *Mater. Today* **18** 252
[2] Etacheri V, Marom R, Elazari R, Salitra G and Aurbach D 2011 *Energy Environ. Sci.* **4** 3243
[3] Alias N and Mohamad A A 2015 *J. Power Sources* **274** 237
[4] Tarascon J M and Armand M 2001 *Nature* **414** 359
[5] Wang Y, Liu B N, Zhou G, Nie K H, Zhang J N, Yu X Q and Li H 2019 *Chin. Phys. B* **28** 068202
[6] Xia R S, Cui Z H, Liu B Q, Guo X X and Zhao J T 2010 *Chin. Phys. Lett.* **27** 076102
[7] Choi J W, Cheruvally G, Ahn H J, Kim K W and Ahn J H 2006 *J. Power Sources* **163** 158
[8] Butala M M, Mayo M, Doan-Nguyen V V T, Lumley M A, Göbel C, Wiaderek K M, Borkiewicz O J, Chapman K W, Chupas P J, Balasubramanian M, Laurita G, Britto S, Morris A J, Grey C P and Seshadri 2017 *Chem. Mater.* **29** 3070
[9] Wang L, Wu Z, Zou J, Gao P, Niu X, Li H and Chen L 2019 *Joule* **3** 2086
[10] Zhu Y, Fan X, Suo L, Luo C, Gao T and Wang C 2016 *ACS Nano* **10** 1529
[11] Zou J, Zhao J, Wang B, Chen S, Chen P, Ran Q, Li L, Wang X, Yao J, Li H, Huang J, Niu X and Wang L 2020 *ACS Appl. Mater. Interfaces* **12** 44850
[12] Lu B, Ning C, Shi D, Zhao Y and Zhang J 2020 *Chin. Phys. B* **29** 026201
[13] Wu F, Pollard T. P, Zhao E, Xiao Y, Olguin M, Borodin O and Yushin G 2018 *Energy Environ. Sci.* **11** 807
[14] He J, Chen Y and Manthiram A 2018 *Energy Environ. Sci.* **11** 2560
[15] He Y, Qiao Y, Chang Z, Cao X, Jia M, He P and Zhou H 2019 *Angew. Chem. Int. Ed.* **58** 11774
[16] Hu Z, Zhang K, Zhu Z, Tao Z and Chen J 2015 *J. Mater. Chem. A* **3** 12898
[17] Zhang C, Cui L, Abdolhosseinzadeh S and Heier J 2020 *InfoMat* **2** 613
[18] Li S, Jiang M, Xie Y, Xu H, Jia J and Li J 2018 *Adv. Mater.* **30** e1706375
[19] Zhou G, Tian H, Jin Y, Tao X, Liu B, Zhang R, Seh Z W, Zhuo D, Liu Y, Sun J, Zhao J, Zu C, Wu D S, Zhang Q and Cui Y 2017 *Proc. Natl. Acad. Sci. USA* **114** 840
[20] Sun K, Cama C A, DeMayo R A, Bock D C, Tong X, Su D, Marschilok A C, Takeuchi K J, Takeuchi E S and Gan H 2016 *J. Electrochem. Soc.* **164** A6039
[21] Zeng P, Li J, Ye M, Zhuo K and Fang Z 2017 *Chem. Eur. J.* **23** 9517
[22] Zou G, Hou H, Ge P, Huang Z, Zhao G, Yin D and Ji X 2018 *Small* **14** e1702648
[23] Palaniselvam T, Biswal B. P, Banerjee R and Kurungot S 2013 *Chem. Eur. J.* **19** 9335
[24] Kresse G and Furthmüller J 1996 *Comput. Mater. Sci.* **6** 15
[25] Kresse G and Furthmüller J 1996 *Phys. Rev. B* **54** 11169
[26] Kresse G and Joubert D 1999 *Phys. Rev. B* **59** 1758
[27] Perdew J. P, Burke K and Ernzerhof M 1996 *Phys. Rev. Lett.* **77** 3865
[28] Zhou Y, Yan D, Xu H, Feng J, Jiang X, Yue J, Yang J and Qian Y 2015 *Nano Energy* **12** 528
[29] Wu N, Lei Y, Wang Q, Wang B, Han C and Wang Y 2017 *Nano Research* **10** 2332
[30] Liu J, Wen Y, Wang Y, van Aken P A, Maier J and Yu Y 2014 *Adv. Mater.* **26** 6025
[31] Lu Z, Zhai Y, Wang N, Zhang Y, Xue P, Guo M, Tang B, Huang D, Wang W, Bai Z and Dou S 2020 *Chem. Eng. J.* **380** e122455
[32] Jin A, Kim M J, Lee K S, Yu S H and Sung Y E 2019 *Nano Research* **12** 695
[33] Zang R, Li P, Guo X, Man Z, Zhang S, Wang C and Wang G 2019 *J. Mater. Chem. A* **7** 14051
[34] Gong W, Lin Y, Chen C, Al-Mamun M, Lu H. S, Wang G, Zhang H and Zhao H 2019 *Adv. Mater.* **31** e1808341
[35] Shao M, Cheng Y, Zhang T, Li S, Zhang W, Zheng B, Wu J, Xiong W W, Huo F and Lu J 2018 *ACS Appl. Mater. Interfaces* **10** 33097
[36] Son S B, Yersak T A, Piper D M, Kim S C, Kang C S, Cho J S, Suh S S, Kim Y U, Oh K H and Lee S H 2014 *Adv. Energy Mater.* **4** e1300961
[37] Tan R, Yang J, Hu J, Wang K, Zhao Y and Pan F 2016 *Chem. Commun.* **52** 986
[38] Diao Y, Xie K, Xiong S and Hong X 2013 *J. Power Sources* **235** 181
[39] Sun W, Li Y, Liu S, Guo Q, Zhu Y, Hong X, Zheng C and Xie K 2020 *Nano Research* **13** 2143